catalysts

Supplementary Materials

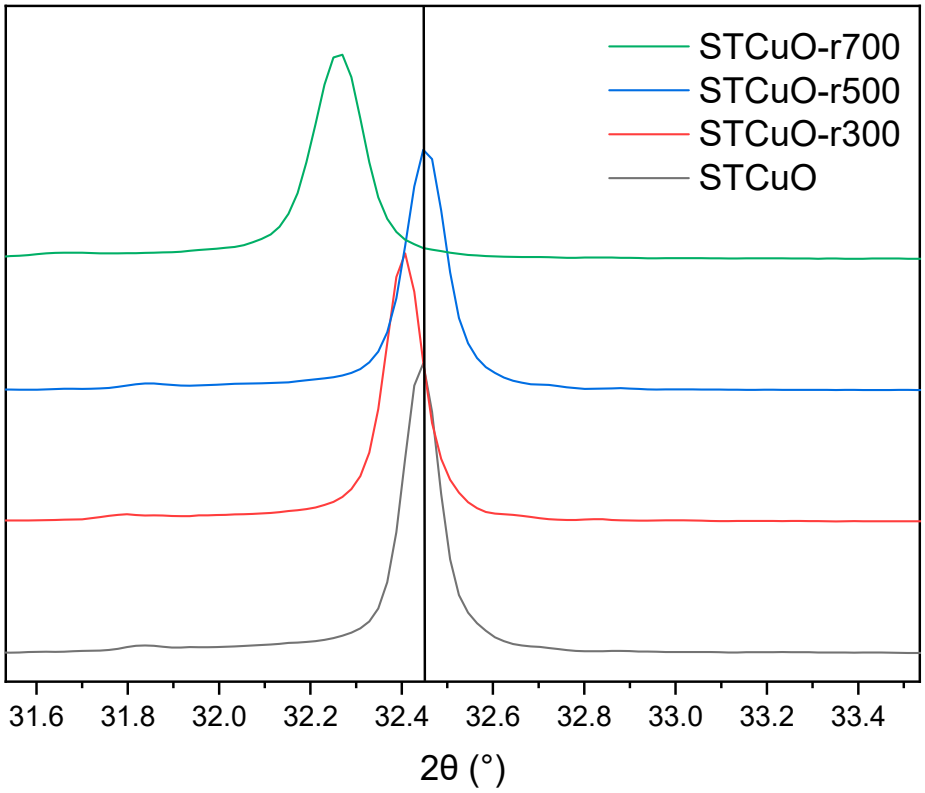

Figure S1. XRD enlargement of various Cu-doped samples. A significant shift can be observed in STCuO-r700, corresponding to Cu incorporation as the result of Ti reduction: a cell expansion is caused by Ti^{3+} formation, that further leads to the diffusion of Cu^{2+} ions in the bulk.

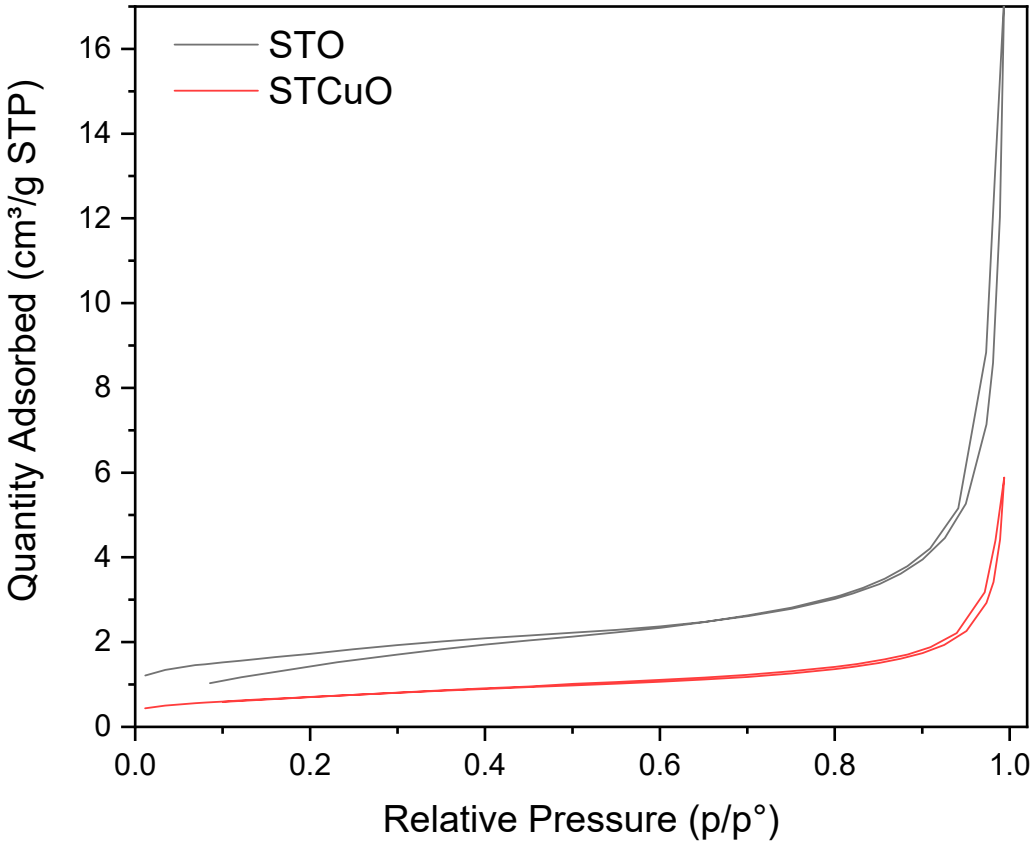

Figure S2. N_2 adsorption-desorption isotherms analyzed with BET method for STO (black) and STCuO (red).

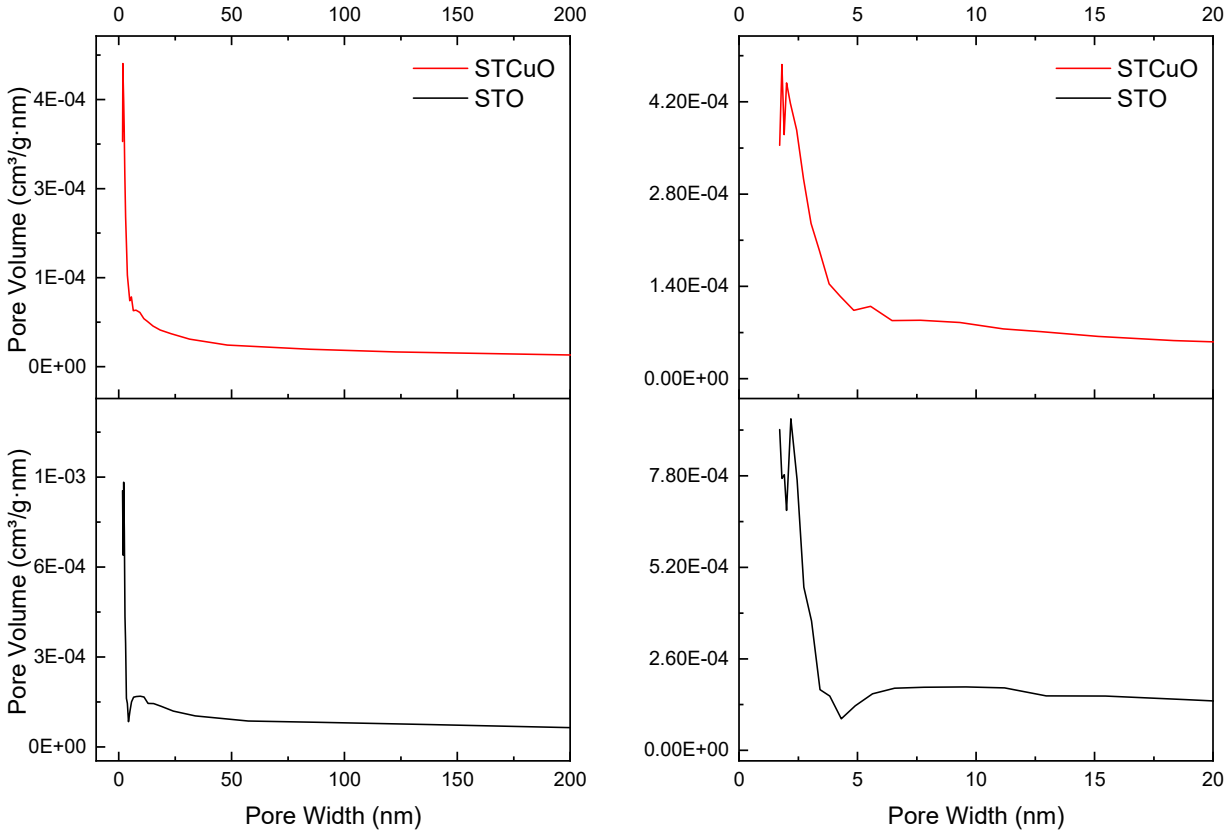

(a) **(b)**

Figure S3. Pore Volume/Pore width curve for STO and STCuO (a), with an enlargement at low dimensions (b).

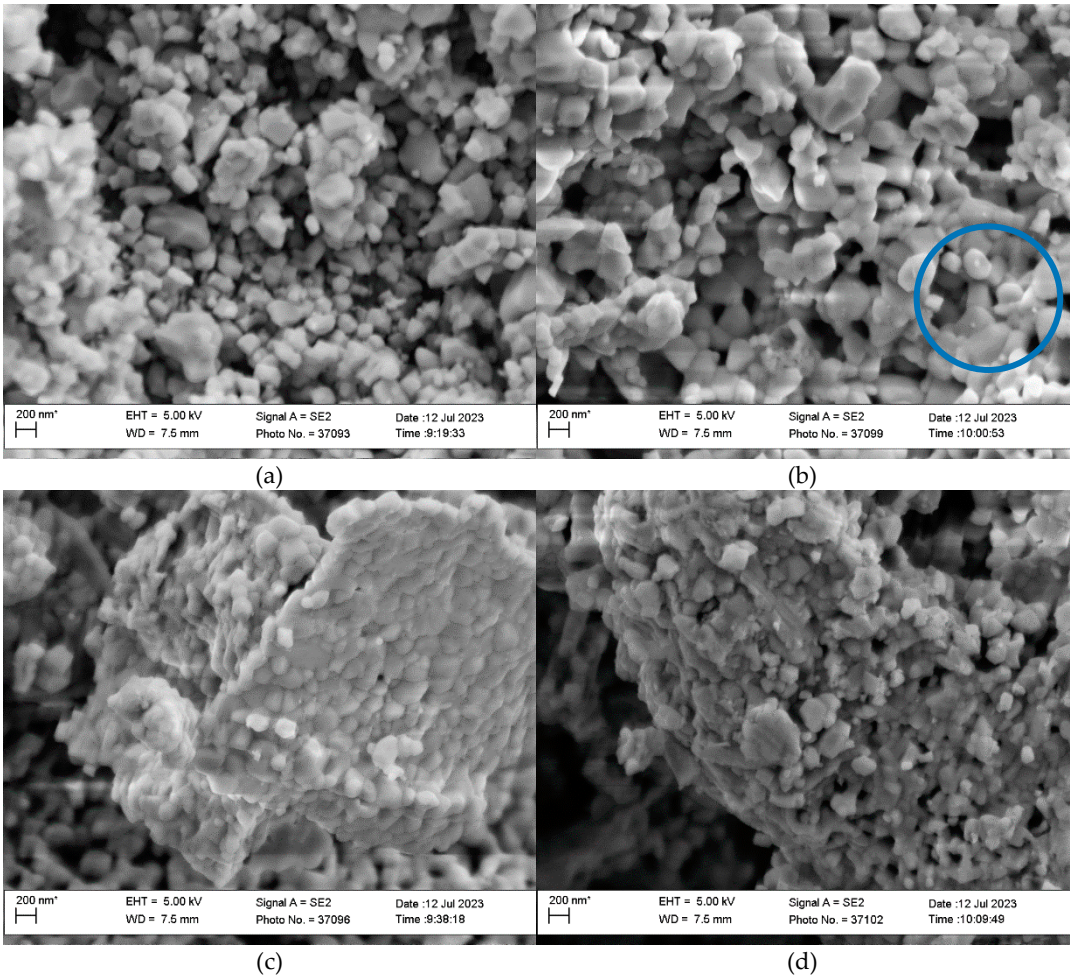

Figure S4. SEM images of as prepared STCuO (a) and reduced samples: STCuO-r300 (b), STCuO-r500 (c) and STCuO-r700 (d); a progressive change in morphology is observed, with grain growth and a porosity decrease. For STCuO.r300, the presence of nanoparticles, ascribed as Cu aggregates, is observed (in circle).

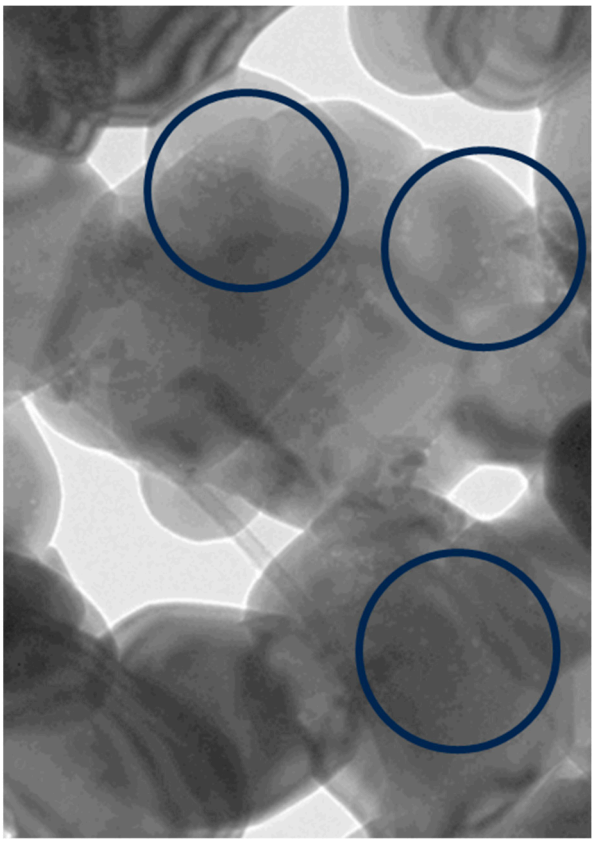

Figure S5. Enlargement of TEM image of STCuO-r300. Small nanoparticles can be observed, ascribed as Cu nanoparticles on the perovskite grains.

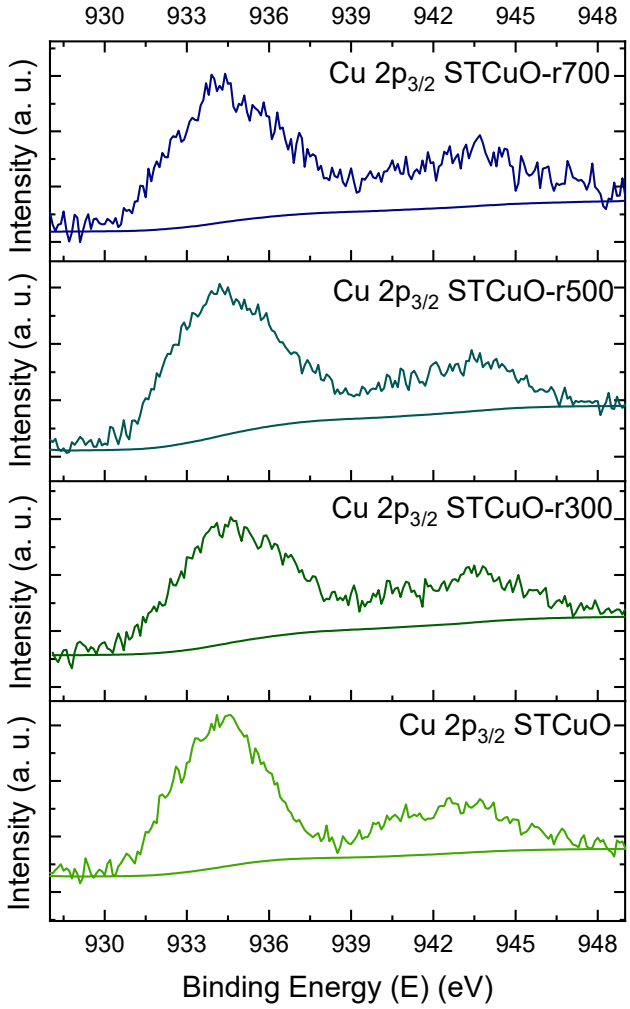

Figure S6. High resolution XPS spectra of Cu $2p_{3/2}$ region.

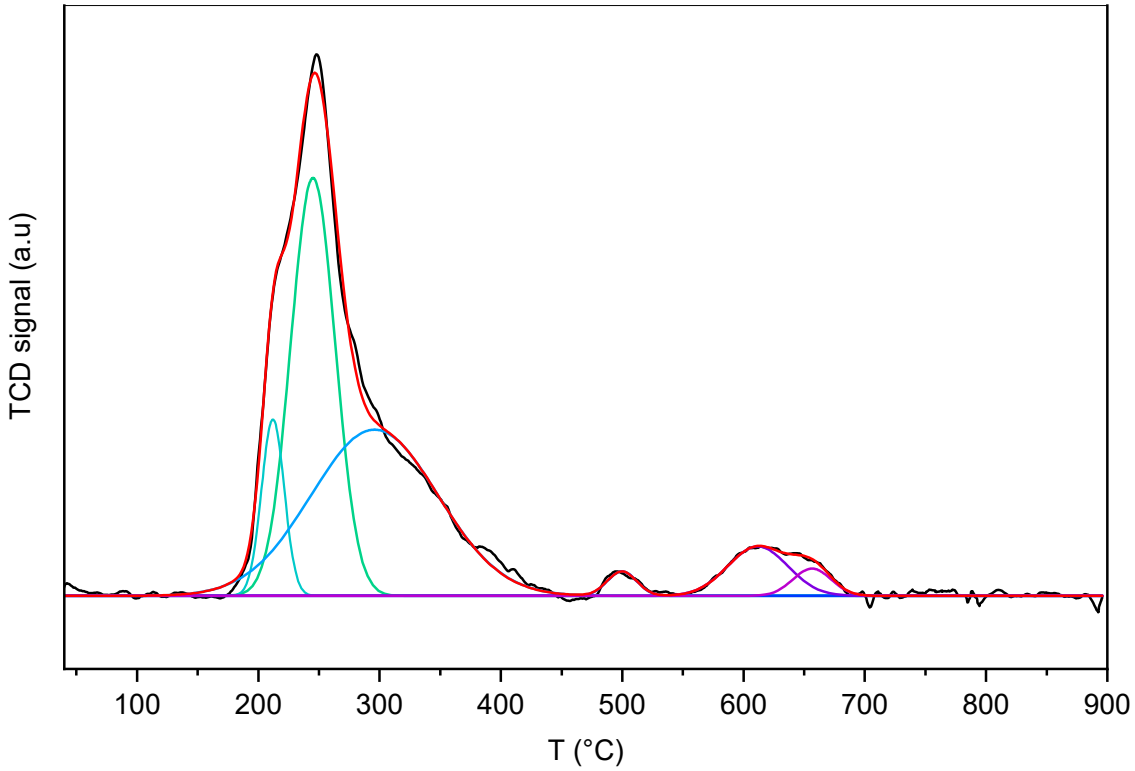

Figure S7. Peak fit of STCuO H_2-TPR.

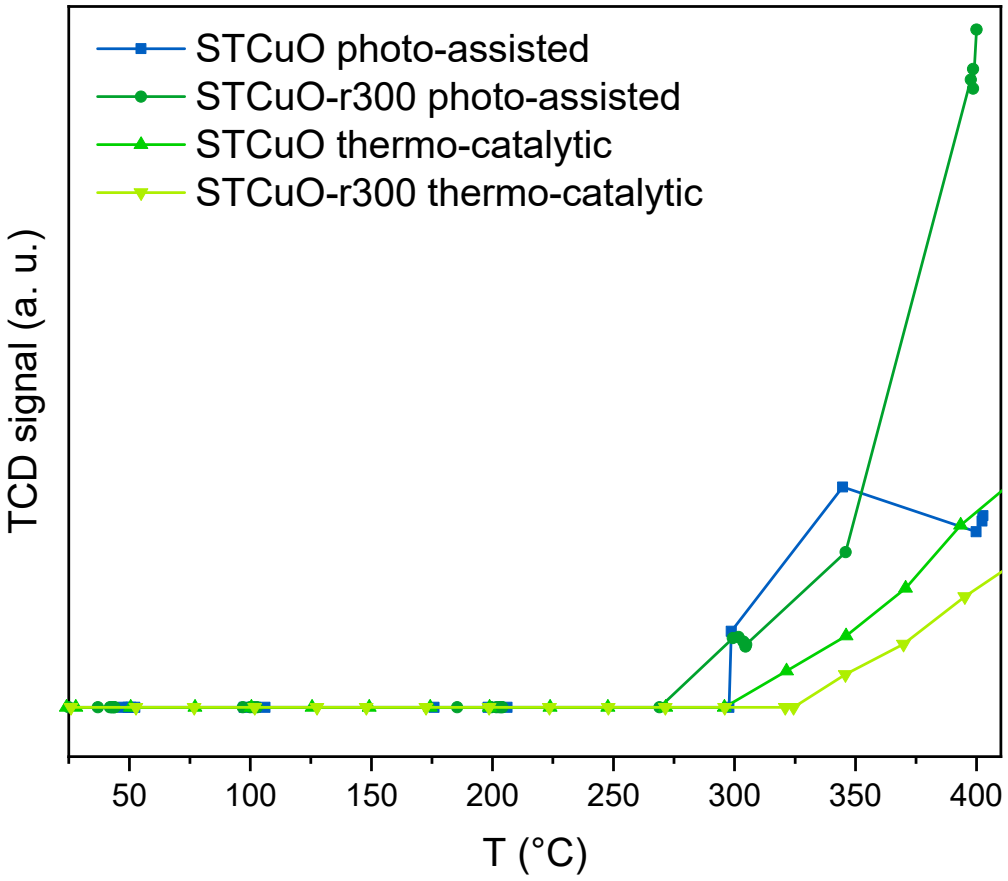

Figure S8. CO production in STCuO and STCuO-r300 both in dark and photo-assisted conditions.

Table S1. Surface elemental composition of the samples discussed in this work.

Sample	Element			
	O	**Ti**	**Sr**	**Cu**
STO	66.17	18.61	15.22	-
STCuO	64.51	16.43	14.92	4.14
STCuO-r300	66.68	15.14	14.06	4.02
STCuO-r500	65.53	16.53	14.33	3.61
STCuO-r700	67.83	14.79	17.31	2.17